SECOND QUARTERLY REPORT ON THE CONSTRUCTION AND TEST OF A DUAL PATCH MULTI-ELEMENT RADIANT COOLER

R.V. Annable

ITT-Aerospace/Optical Division
Electro-Optical Operations
Fort Wayne, Indiana 46803

March 1971

Interim Report for Period 17 December 1970 to 17 March 1971

Prepared for

GODDARD SPACE FLIGHT CENTER
Greenbelt, Maryland 20771

1. Report No.	2. Government Accession No.	3. Recipient's Catalog No.
4. Title and Subtitle SECOND QUARTERLY REPORT ON THE CONSTUCTION AND TEST OF A DUAL PATCH MULTI-ELEMENT RADIANT COOLER		5. Report Date March 1971
		6. Performing Organization Code
7. Author(s) R. V. Annable		8. Performing Organization Report No.
9. Performing Organization Name and Address ITT Aerospace/Optical Division Electro-Optical Operations Fort Wayne, Indiana 46803		10. Work Unit No.
		11. Contract or Grant No. NAS5-21132
		13. Type of Report and Period Covered Interim 17 Dec. 1970-17 Mar. 1971
12. Sponsoring Agency Name and Address Goddard Space Flight Center Greenbelt, Maryland 20771 I. L. Goldberg, Code 731		14. Sponsoring Agency Code
15. Supplementary Notes		

16. Abstract This report covers the second quarter of the construction and test phase of the program. All mechanical parts were fabricated, and the dual patch compartment was assembled. A dual patch passed sinusoidal vibration tests at 20 G's. The construction and installation of the cooler test equipment was completed. The temperatures of the cone and second (90K) patch were recalculated to reflect small changes in the design. The study of cone surface properties was continued with a consideration of the sensitivity of cone designs to diffuse wall reflections. Semi-quantitative data on the infrared absorption of ice was used to re-evaluate the effects of residual outgassing. Experimental measurements confirmed theoretical predictions on the radiative decoupling between low-emissivity surfaces.

17. Key Words		18. Distribution Statement	
19. Security Classif. (of this report)	20. Security Classif. (of this page)	21. No. of Pages	22. Price

PREFACE

This report covers the second quarter of the contract's second phase, the construction and test of a dual patch multi-element radiant cooler. The soundness of the mechanical design was verified by sinusoidal vibration tests on the dual patch assembly. Data on the properties of ice at cryogenic temperatures showed that it has about the same absorption coefficient as liquid water at 12 μm but a much larger coefficient at 3 μm. Theoretical studies showed that the cone design used in the radiant cooler is relatively insensitive to diffuse wall reflections. Experimental studies showed that close-spaced, low-emissivity surfaces have the theoretically expected radiative insulation factor.

TABLE OF CONTENTS

LIST OF ILLUSTRATIONS

LIST OF TABLES

1.0 INTRODUCTION

The emphasis during the second quarter of the construction and test phase of the program was on the fabrication and assembly of the breadboard cooler and test equipment. The fabrication of all cooler parts was completed, and the patch compartment of the cooler was assembled (Section 2.0). A dual patch successfully completed sinusoidal vibration tests at a level of 20 G's (Appendix). All of the test equipment was constructed, assembled, and installed (Section 3.0).

The temperatures of the cone and second (90K) patch were recalculated for lower values of insulation factor and for several small changes in the cooler design (Section 4.0). The study of cone surface properties showed that the cone design is relatively insensitive to a component of diffuse wall reflection (Section 5.0). Semi-quantitative data on the infrared absorption of ice were used to re-evaluate the previous study of residual outgassing (Section 6.0).

Experimental measurements showed that close-spaced, low-emissivity surfaces provide the theoretically expected radiative decoupling (Section 7.1). That is, they have an insulation factor of approximately $2/\epsilon$, where ϵ is the hemispherical emissivity of either surface. In addition, the experimental equipment was modified so that it could also be used to determine the hemispherical emissivity of low-emissivity surfaces (Section 7.2).

2.0 COOLER CONSTRUCTION

The fabrication of all the parts for the breadboard cooler was completed during the second quarter. The patch compartment consisting of the two patches, their supports and electrical leads, and the insulation below the patches was assembled. The detailed mechanical designs of the two patches are shown in Figures 2-1 and 2-2. The supports and electrical leads are listed in Section 4.0.

A dual patch assembly was sinusoidally vibrated as described in Section 6.0 of the first quarterly report for Phase II. One of the four support tubes to the first (120K) patch was found to be loose after completion of the roll axis vibration. The tube was re-cemented and the pitch axis vibration completed without incident. The total vibration time for the three axis was about 30 minutes. Resonant frequencies were noted in each axis as shown in Table 2-1. The complete test report is reproduced in the appendix.

Table 2-1

Dual Patch Assembly Resonant Frequencies

Axis	Frequencies (Hz)
Yaw	105
Roll	30, 85
Pitch	80, 100

A multiple punch for multilayer insulation was constructed. The punch provides 1/8-inch diameter holes on 1 inch centers to aid in the outgassing of insulation blankets (see Section 3.4 of the first quarterly report for phase 2). There is a total of 48 punches in a 6×8 array.

7

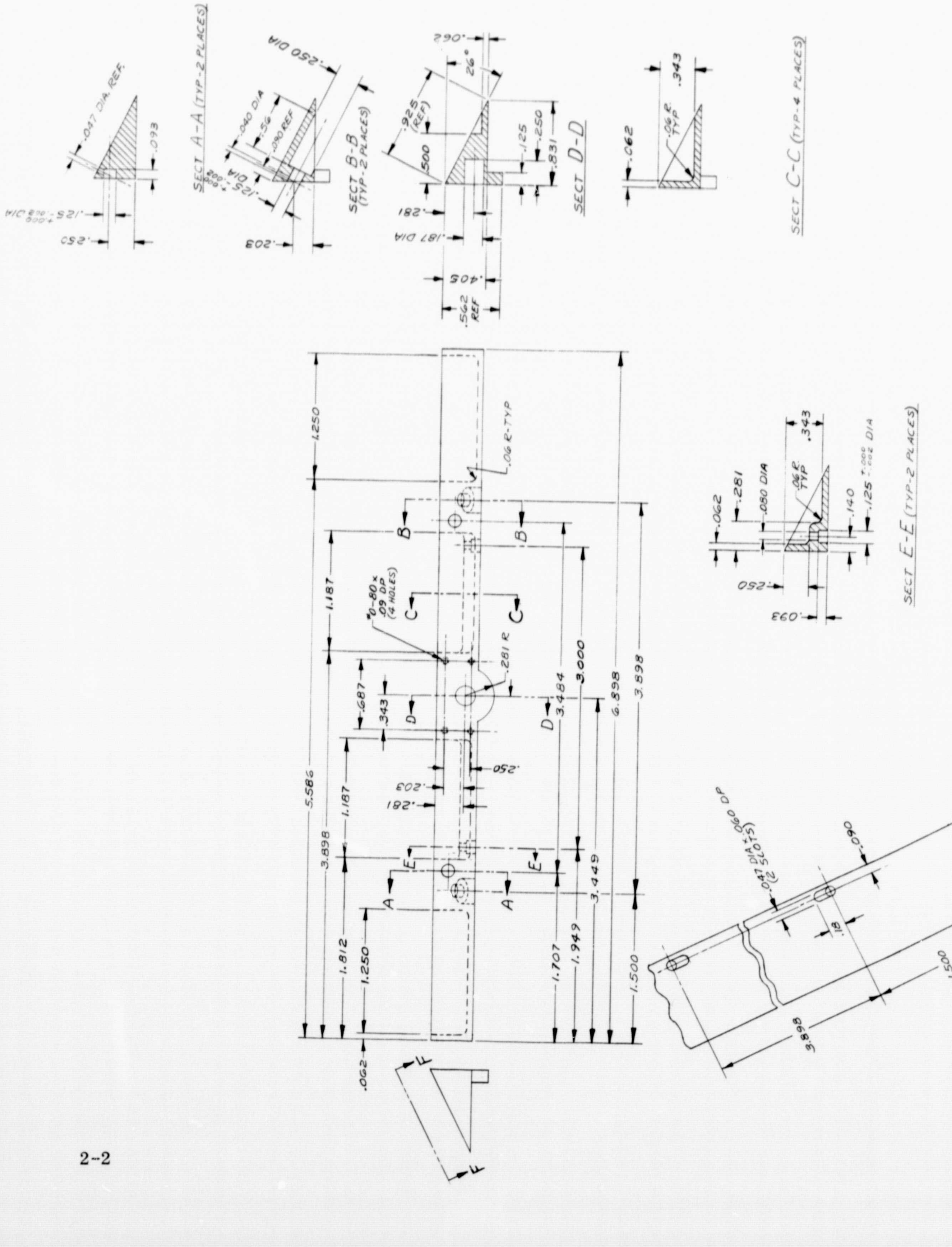

Figure 2-1. Detailed Design of Detail 1 (100X)

3.0 COOLER TESTING

The equipment needed for thermal testing of the breadboard cooler was completed during the second quarter. The space target and liquid nitrogen shroud were constructed and installed in the space chamber as described in Section 7.0 of the design study report (July 1970). The Norelco A-20 helium refrigerator and the temperature regulated baseplate described in the design study report were available from Contract NAS5-1049[illegible]. The temperature of the shroud will be measured by means of a calibrated platinum resistance thermometer and the temperature of the copper space target with a chromel-constantan differential thermocouple referenced to the resistance thermometer.

The layout of the test equipment rack is shown in Figure 3-1. The integrating digital voltmeter (Section 3.0 of the September 1970 monthly report) is used to measure the outputs of the resistance thermometer bridges, differential thermocouples, and heater power supplies. The milliammeters used to measure heater and bias current have an accuracy of ±2 percent of full scale. The heaters required for initial outgassing and for cooler testing are described in Section 5.0 of the first quarterly report.

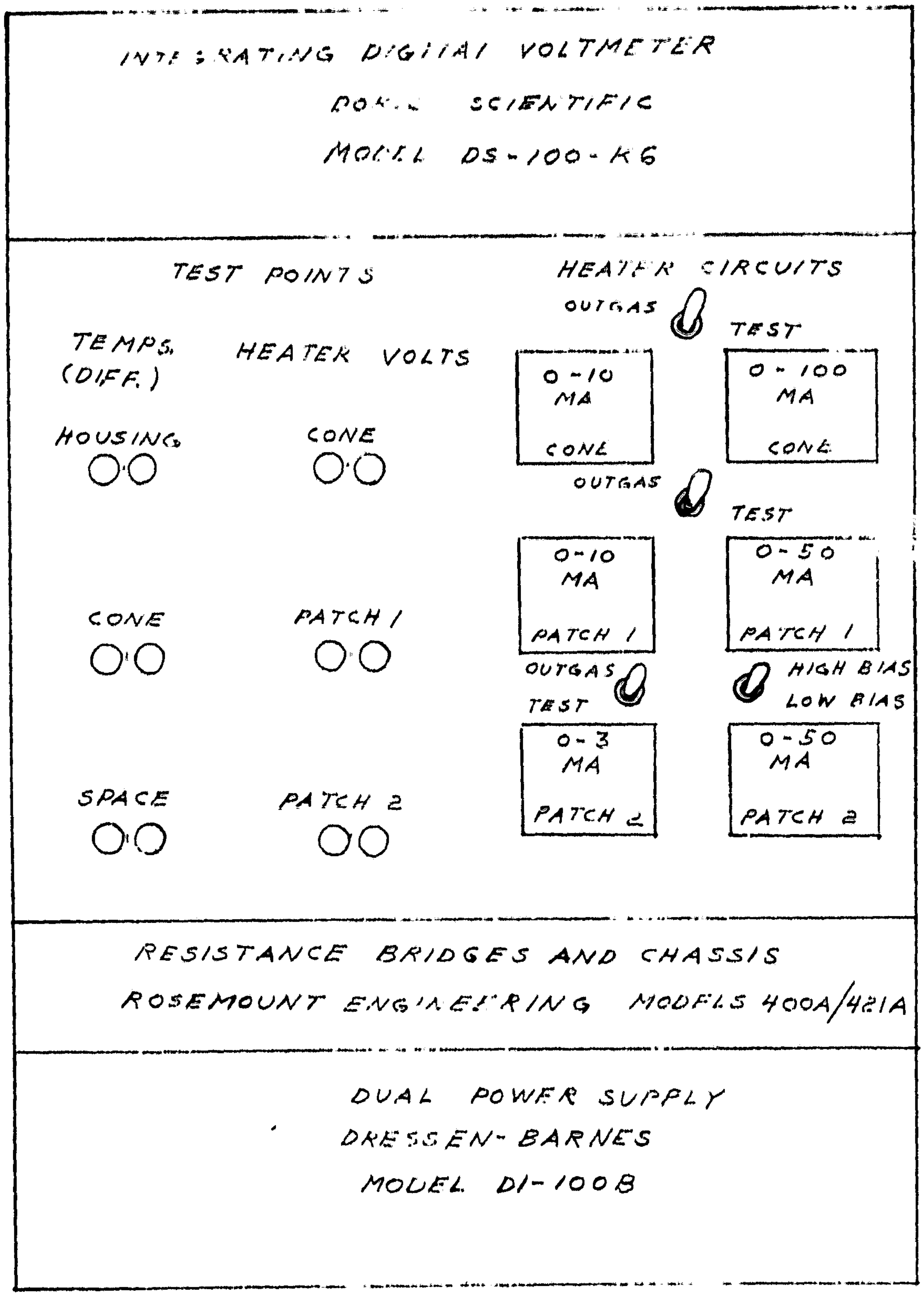

Figure 3-1 Test Equipment Rack

4.0 RECALCULATION OF TEMPERATURES IN THE MULTI - ELEMENT RADIANT COOLER

The temperatures of the cone and second (90K) patch were recalculated for the following conditions:

a. Cone insulation factors of 80 and 60.

b. Patch insulation factors of 100, 80, and 60.

c. Actual connections between cooler members.

d. Patch cold trap in place of anti-frost enclosure.

e. Correct value of radiative coupling factor (ϵ_{pc}) between second patch and cone.

f. Patch emissivity of 0.92.

g. Insulated patch area (A_i) of 8.89 in^2.

Except for the insulation factors, nominal values for thermal properties were used in the calculations (see Sections 3.0 and 4.0 of the design study report). In addition, the nominal housing temperature of 25 degrees C was used.

Tests on both multilayer insulation fixtures and actual radiant coolers indicate that insulation factors in the range of 80 to 100 between the housing and outer cone structure are difficult, if not impossible, to achieve. The realization of high insulation factors between the cone structure and rear of the patch is also likely to prove difficult. We have therefore reduced the insulation factors to the ranges listed above.

The cold trap attached to the patch increases the radiative input (Φ_o) through the optical opening because it increases the receiving area attached to the patch. The values of ϵ_{pc} for area 2 (patch 2) given for design IA (III A) in Table 37 (p. 5-4) of the design study report are in error. This is a result of the incorrect value of the view factor ($F_{p-m(1)}$) given in Table 36 for the view from the patch to the first-reflection image of the cone mouth. The correct values are shown in Table 4-1.

Table 4-1

Corrected Values of Cone Coupling
Factors from Second Patch

$F_{p-m(1)}$ = 0.29648

ϵ_{pc} (0.05) = 0.02095

ϵ_{pc} (0.07) = 0.0292

The actual connections between cooler members are listed in Tables 4-2, 4-3 and 4-4.

Table 4-2

Connections Between Housing and Cone

Quantity	for	Dia. (in.)	Length (in.)	Material
2	Support	1/4X3/16	1.51	Synthane
1	Support	1/4X3/16	1.66	
2	Support	1/4X1/8	3.00	
15	InAs	$3X10^{-3}$	1.51	Chromel
4	Patch Heat	$3X10^{-3}$	1.66	
1	Cone Diff. Temp.	$3X10^{-3}$	1.66	
1	Cone Diff. Temp.	$3X10^{-3}$	1.66	Constantan
12	Temp. Sensors	$2X10^{-3}$	1.66	Nickel
2	Cone Heat	$2X10^{-3}$	1.66	
5	HgCdTe	$2X10^{-3}$	1.51	

$K_c = 6.73 \times 10^{-4}$ W/K

Table 4-3

Connections Between Cone and Patch 1

Quantity	for	Dia. (in.)	Material
15	InAs	$3X10^{-3}$	Chromel
4	Patch Heat	$3X10^{-3}$	Chromel
8	Patch Temp.	$3X10^{-3}$	Chromel
5	HgCdTe	$2X10^{-3}$	Nickel
4	Support	1/ 8X3/32	Synthane

All lengths = 1.6 inches, $K_{p1} = 1.71X10^{-4}$ W/K

Table 4-4

Connections Between Patches

Quantity	for	Dia. (in.)	Material
5	HgCdTe	$2X10^{-3}$	Nickel
4	Patch Temp.	$3X10^{-3}$	Chromel
2	Patch Heat	$3X10^{-3}$	Chromel
2	Support	1/8X3/32	Synthane

All lengths = 1.2 inches; $K_{p2} = 1.126X10^{-4}$ W/K

The revised temperatures for the cone and second patch are listed in Table 4-5. The notation used in the table is

s_i (c) = cone insulation factor
s_i (p) = patch 2 insulation factor
t_c = cone temperature
t_p = patch temperature

The results are for a housing temperature of 25 degrees C and nominal values of emissivities and absorptivities (gold cone). For an insulation factor of 60, the cone temperature is 6.3 K above the previously calculated nominal value of 173.5K (Table 7 of the design study report). The previously calculated nominal value of patch 2 temperature was 84.2K (Table 26 of the design study report). All calculations of patch 2 temperature are for a patch 1 temperature of 120K. The cold trap on patch 2 is made of polyethylene, which is about the same absorptivity (0.6) as germanium. However, it increases the collecting diameter for radiation from the optical opening to 0.6 inch. The value of Φ_0 for a cone at 175K is then 2.8 milliwatts.

The joule heat on patch 2 is assumed to be 2 milliwatts. In addition, the rear patch area (A_i) being insulated was increased to the value of patch 1 (8.894 in^2).

Table 4-5

Revised Cone and Patch 2 Temperature

s_i (c)	t_c (K)	s_i (P)	t_{p2} (K)
80	172.6	100	87.6
80	172.6	80	88.7
80	172.6	60	90.4
60	179.8	100	89.5
60	179.8	80	90.7
60	179.8	60	92.6

5.0 CONE SURFACE PROPERTIES

The preliminary experimental determination of the effective cone wall emissivity ϵ_c in a 45 degree test cone was reported in the first quarterly report (Section 4.2). The upper limit to ϵ_c was estimated to be 0.048 for vacuum deposited aluminum. The average surface flatness of the nickel plated walls was about 17 wavelengths of visible light. To obtain a comparable performance in the radiant cooler cones for the SCMR and ATS-F VHRR in terms of the level of diffuse reflectance requires a finer optical finish (~8 wavelengths). The test cone is less sensitive to deviations from specular reflectance because of the larger view to cold space from the cone walls. On the other hand, the multi-element radiant cooler (MERC) has a view from the cone to space nearly as large as the test cone. As a result, the surface finish required for the same performance is comparable to that of the test cone (~15 wavelengths).

The test cone is more sensitive than the other three designs to directional emissivity effects (Section 2.1 of the first quarterly report). Incidence angles at the cone walls for patch radiation are limited to the range from 45 degrees to 90 degrees in the test cone. On the other hand, patch rays in the other design either go down to or approach normal incidence (10 degrees, 7.5 degrees, and 0 degrees). Thus cone walls finished to obtain the same cooler specularity as in the test cone should result in a lower value of ϵ_c because of the decrease in average cone wall incidence angle.

A non-specular component of reflection at the cone walls increases the apparent specular emissivity ϵ_c, as discussed in Section 2.2 of the first quarterly report. We will approximate the non-specular component as pure diffuse (Lambertian). Based on the specular model used in the experimental analysis, the presence of patch radiation returned to the patch and the increase in patch radiation absorbed in the cone walls as a result of diffuse reflectivity are both interpreted as increases in ϵ_c. For diffuse reflection at the cone walls, the increase is

$$M = 1+(1-\epsilon_h)\, f+(1\,\epsilon_h)^{2} f^{2}+\ldots = \frac{1}{1-(1-\epsilon_h)\, f}$$

where ϵ_h is the hemispherical emissivity and f the fraction of patch radiation diffusely reflected at the cone walls that does not reach the space target (cone mouth).

The fraction f is given by

$$f = F_{cc} + F_{cp} = 1-F_{cs},$$

where

F_{ij} = view factor from i to j
c = cone walls
p = patch opening
s = visible space target (cone mouth).

Using the relationships (reciprocity and sum of view factors equals unity)

$$F_{cs} = \frac{A_s}{A_c} F_{sc}$$

$$F_{sc} = 1 - F_{sp}$$

$$F_{sp} = \frac{A_p}{A_s} F_{ps},$$

this becomes

$$1 - F_{cs} = \frac{1}{A_c} (A_c - A_s - A_p F_{ps}),$$

where A_k is the area of surface k.

For ϵ_h much less than unity, we have

$$M = \frac{1}{1 - f} = \frac{1}{F_{cs}}$$

Neglecting directional effects, a hemispherical emissivity ϵ_h on a cone wall surface at which a fraction g of the reflection is diffuse , then results in an effective specular emissivity given by

$$\epsilon_c = \epsilon_h \left[(1-g) + \frac{g}{F_{cs}} \right]$$

Note that for $F_{cs} = 0$, $f = 1$, and $M = \frac{1}{\epsilon_h}$. This is the limiting case of maximum sensitivity to diffuse reflectance (R. V. Annable, Appl. Opt. 9, 185, Section IV). We then have $\epsilon_c = \epsilon_h (1-g)+g$ or $\epsilon_c = \epsilon_h+g$ for g much less than one. The values of $1/F_{cs}$ are given in Table 5-1 for the test cone (TC) and for the other three cooler designs.

Table 5-1

Apparent Cone Wall Emissivity

Increase Produced by Diffuse Reflection

Cone Design	$\frac{1}{F_{cs}}$	Compared With TC
TC	1.366	1
SCMR	2.515	1.841
ATS-F	2.602	1.905
MERC	1.445	1.058

The design values for the test cone are

$$\frac{A_s}{A_c} = \frac{9}{8\sqrt{2}}$$

$$\frac{A_p}{A_c} = \frac{1}{8\sqrt{2}}$$

$$F_{ps} = 0.7173$$

The design values for the other cooler designs were taken from their respective design study reports. The factor F_{ps} is equal to the factor $F_{p-m}(0)$ given in the reports.

The SCMR and ATS-F designs are considerably more sensitive to a diffuse component of reflection than the TC and MERC designs. To obtain the value of ϵ_c obtained in the test cone, it is necessary to maintain the value of $[(1-g) + \frac{g}{F_{cs}}]$ constant by reducing g. The fraction g of diffuse reflection can be related to the surface finish on the cone walls by (See Section 2.2 of the first quarterly report).

$$g = 1-\exp[-(4\pi\sigma/\lambda)^2]$$

where

σ = rms deviation of surface from its mean surface limit (roughness)

λ = wavelength of radiation.

In general, the argument of the exponent is much less than unity, so that the right side of the equation may be expanded to give

$$g = 1 - [1-(\frac{4\pi\sigma}{\lambda})^2 + \frac{1}{2}(\frac{4\pi\sigma}{\lambda})^4 - \cdots]$$
$$g = (\frac{4\pi\sigma}{\lambda})^2 \cdots$$

The required surface finish (as measured by σ) is then proportional to the square root of g. We may assume a linear relationship between σ and the surface flatness (ibid). The resultant surface finishes needed in the other designs for an effective emissivity equal to that of the test cone are listed in Table 5-2. It is assumed that directional effects are not present and that the evaporated materials have the same properties.

Table 5-2

Required Surface Flatness

For Equal Values Of Effective

Wall Emissivity

Design	$(g/g_{TC})^{1/2}$	Surface Flatness (Visible Wavelengths)
SCMR	0.492	~ 8
ATS-F	0.477	~ 8
MERC	0.907	~ 15

In the above analysis, we did not distinguish between diffusely reflected radiation going to the patch and going to the cone. In addition, we did not account for multiple reflections in the case of specular wall reflection. These refinements have little effect on the calculations for the test cone in which the view factor from cone to patch is very small and in which there are no multiple specular reflections.

For specularly reflecting cone walls, the radiative coupling factor between the patch and cone is

$$\epsilon_{pc} = 1 - F_{p-m}(n)(1-\epsilon_h)^n$$

where

$F_{p-m}(n)$ = view factor from patch to images of cone mouth formed by n specular wall reflections

ϵ_h = hemispherical emissivity of cone walls.

For $\epsilon_h^2 << 1$, we have

$$(1 - \epsilon_h)^n = 1 - n\epsilon_h + \frac{n(n-1)}{2}\epsilon_h^2 - \ldots$$

And for $\epsilon_h (n-1) << 2$, i.e., $\epsilon_h << 1$ when $n << 3$, this becomes

$$(1 - \epsilon_n)^n = 1 - n\epsilon_h.$$

Then, using

$$\Sigma F_{p-m}(n) = 1,$$

we obtain

$$S = \frac{\epsilon_{pc}}{\epsilon_h} = \Sigma n F_{p-m}(n)$$

Values of this ratio are given in Table 5-3 for the four radiant cooler designs of interest.

Table 5-3

Ratio of Effective to Hemispheric Emissivity for Specular Reflection

Design	$F_{p-m(1)}$	$F_{p-m(2)}$	$\Sigma nF_{p-m(n)}$
TC	0.2827	0	0.2827
SCMR	0.5078	0.1691	0.8460
ATS-F	0.5170	0.1613	0.8396
MERC*	0.3653	0.673	0.4999

*Total patch opening.

The view factors from the patch to space (cone mouth) and from the patch to cone are listed in Table 5-4.

Table 5-4

View Factors from the Patch

Design	$F_{ps} = F_{p-m(0)}$	$F_{pc} = 1 - F_{ps}$
TC	0.7173	0.2827
SCMR	0.3231	0.6769
ATS-F	0.3217	0.6783
MERC	0.5674	0.4326

For diffusely reflecting cone walls, we will first consider the fraction of patch radiation absorbed in the cone walls (i.e., the patch-cone radiative coupling factor). It is given by

$$\epsilon_{pc} = \epsilon_h F_{pc} [1 + (1 - \epsilon_h) F_{cc} + (1 - \epsilon_h)^2 F_{cc}^2 + \cdots]$$

$$= \frac{\epsilon_h F_{pc}}{1 - (1 - \epsilon_h) F_{cc}}$$

where F_{cc} is the view factor from the cone to itself. For $\epsilon_h \ll 1$, we obtain

$$D = \frac{\epsilon_{pc}}{\epsilon_h} = \frac{F_{pc}}{1 - F_{cc}}$$

Secondly, consider the patch radiation returned to the patch as a result of diffuse reflection at the cone walls. The fraction is given by

$$r = F_{pc} \cdot F_{cp} [1 + (1 - \epsilon_h) F_{cc} + \cdots]$$

$$r = \frac{F_{pc} F_{cp}}{1 - (1 - \epsilon_h) F_{cc}}$$

For $\epsilon_h \ll 1$, this becomes

$$r = \frac{F_{pc} \cdot F_{cp}}{1 - F_{cc}}$$

Values of the view factors are given in Table 5-5 together with 1-r, the efficiency of patch emission in the presence of diffusely reflecting cone walls.

Table 5-5

Efficiency of Patch Emission

for Diffuse Cone Reflection

Design	F_{pc}	F_{cp}	$F_{pc} \cdot F_{cp}$	1 - r	F_{cc}
TC	0.2827	0.02499	0.007065	0.99067	0.2429
SCMR	0.6769	0.04901	0.03317	0.92573	0.5534
ATS - F	0.6783	0.05593	0.03794	0.91381	0.5598
MERC	0.4326	0.1472	0.06368	0.92414	0.1606

If the radiative input to the patch from the cone is much larger than the sum of all other thermal loads, the degradation factor produced by diffuse cone wall reflection becomes D/S (1 - r). The vlaues of this ratio are given in Table 5-6.

Table 5-6

Degradation Factor
for Cone Wall Radiative
Coupling

Design	D/S (1 - r)
TC	1.333
SCMR	1.935
ATS-F	2.008
MERC	1.116

It is seen that the ratio for the test cone (TC) is very nearly the same as that given in Table 1 (1.366). The values are lower for the other designs. However, thermal inputs to the patch other than cone wall radiation are generally not negligible compared with wall radiation. The two degradations produced by diffuse wall reflection cannot then be combined into a single factor.

Finally, diffuse cone wall reflection can produce a coupling between external sources and the cold patch that is not present for specular reflection. This is an especially important consideration when direct sunlight irradiates the cone mouth as in the ATS-F cooler during about 2 months of the year. The external thermal loads are generally simulated by heaters during cooler tests. A separate chamber test is therefore necessary to determine the source-patch coupling produced by non-specular reflections in a given cooler cone.

6.0 ANTI-FROST DESIGN

The signal attenuation produced by ice accumulated from the residual outgassing of multilayer insulation has already been studied (Ref. 3). We calculated the time needed to produce an ice thickness that attenuates the signal by 10 percent. This was done for the maximum absorption coefficient in two wavelength bands of interest (those covered by InAs and HgCdTe detectors). However, the calculation was based on the absorption coefficients for liquid water rather than ice. That data for ice (Ref. 1) shows that this is a good approximation in the vicinity of 12 μm but a poor one in the vicinity of 3 μm.

Hexagonal (ordinary) ice crystallizes at temperatures above about -80 degrees C (193K (Ref. 2)). Crystallization at lower temperatures produces cubic ice. The absorption curves given in reference 1 are for hexagonal ice at -30 degrees C (243K) and -175 degrees C (98K). In the latter case, the ice was formed above -80 degrees C and then cooled to -175 degrees C. The initial ice condensed on a patch in a radiant cooler will be hexagonal, but most will be cubic. However, because we have no quantitative data on the absorption of cubic ice, we will use the absorption curves for hexagonal ice. Qualitatively, there is little difference in their spectral absorption curves [(Ref. 2), Section 2.3].

Using the hexagonal data in reference 1 (Figure 24), we see that the maximum absorption over the wavelength span from 4.5 to 25 μm occurs in the band from about 10.5 μm to 12.5 μm when the ice is at -175 degrees C. That is, it is essentially coincident with an atmospheric window widely used in radiometry. The most strongly absorbing region in the entire ice spectrum, however, is located in the band for 3.0 to 3.2 μm at about the same ice temperature.

From Figure 24 of reference 1, the transmission is about 0.48 at a wavelength of 11.8 μm for a thickness δ estimated at from 1 to 3 μm (ice at -175 degrees C). The corresponding absorption coefficient is then

$$\alpha = -\frac{1}{\delta}\ \ln T = (2.45 \text{ to } 7.34) \times 10^3 cm^{-1}$$

The value at a thickness of 2 μm is $3.67 \times 10^3 cm^{-1}$. The data for liquid water (Ref. 3) yields an absorption coefficient of $3.00 \times 10^3 cm^{-1}$, which is within the estimated range for ice.

In the vicinity of 3 μm wavelength, the liquid water data yields a maximum absorption coefficient of $4.12 \times 10^3 cm^{-1}$. The ice absorption curve, however, indicates a maximum absorption of greater than $1.83 \times 10^4 cm^{-1}$ at 3.1 μm [(Ref. 1), Figure 25; estimated thickness less that 1 μm]. For $\alpha = 1.83 \times 10^4 cm^{-1}$, $T = 0.90$ at $\delta = 0.576 \times 10^{-5} cm$. The corresponding time at the higher outgassing rate (Ref. 3) is then reduced from 169 to 40 days. The time needed to reach

T ≈ 0.90 in the vicinity of 12 μm wavelenght is about 230 days under the same conditions.

References

1. N. Ockman, The Infrared and Raman Spectra of Single Crystals of Ordinary Ice, Thesis, University of Michigan (1957).

2. N. Ockman, The Infrared and Raman Spectra of Ice, article in technical journal (R. Harber has a copy).

3. R. V. Annable and J. F. Lodder, First Quarterly Report on the Construction and Test of a Dual Patch Multi-Element Radiant Cooler, Contract NAS5-21132, January 1971.

7.0 EXPERIMENTAL STUDIES

To improve the experimental determination of effective cone wall emissivity, the cold space target and insulation below the patch were modified as proposed in the first quarterly report (Section 4.2). The pyramidal target was replaced with a honeycomb cavity array attached directly to the liquid nitrogen reservoir. The stack of multilayer insulation below the patch was replaced by a close-spaced geometry of gold plated aluminum surfaces (rear of patch and facing surface of base). The two patch supports were provided with coaxial low-emissivity shields of gold tape.

A further modification was begun to allow the measurement of the hemispherical emissivity of flat samples in the experimental test setup.

7.1 Radiative Decoupling

The modified equipment was used to determine the effective emissivity of the gold surfaces and therefore the insulation factor of the close-spaced geometry. Based on a set of three experiments, the gold surfaces have an emissivity of 0.042. The corresponding shielding factor is 47.3 between the rear of the patch and the adjacent base (cone structure). The emissivity compares favorably with a previously measured value of 0.048 for a gold plated aluminum surface (Final Report, Part II, on Contract NAS5-11683, 8 April - 15 December, 1969). We may therefore conclude that the close-spaced geometry behaves as expected. The arrangement provides an insulation factor of $2/\epsilon$, where ϵ is the hemispherical emissivity of either surface. Surfaces prepared according to the procedure used on the larger cooler cone for the ITOS radiometer have a hemispherical emissivity of approximately 0.02 (ibid). If such surfaces were used on the facing areas of a close-spaced geometry, they would provide an insulation factor of about 100.

The effects of departures from close-spaced geometry can be estimated from Christiansen's formula (M. Jakob, Heat Transfer, Vol. II, John Wiley & Sons, 1957, p. 5),

$$\frac{1}{\epsilon} = \frac{1}{\epsilon_1} + \left(\frac{1}{\epsilon_2} - 1\right) \frac{A_1}{A_2}$$

where

ϵ = radiative interchange factor or effective emissivity

ϵ_i = emissivity of surface i

A_i = area of surface i

The subscript 1 refers to the inner surface and 2 to the outer. The equation is exact for diffusely reflecting concentric spheres and infinitely long coaxial cylinders. In general, the distance between the two surfaces should not vary much over all the surface. For infinite plane-parallel plates or close-spaced geometry, $A_i / A_2 \rightarrow 1$. We then have

$$\frac{1}{\epsilon} = \frac{1}{\epsilon_1} + \frac{1}{\epsilon_2} - 1$$

This result also holds for specularly reflecting parallel plates, long coaxial cylinders, and concentric spheres. The distinction between diffuse and specular reflection is therefore eliminated for closely spaced surfaces. In terms of shielding factors, the above formula becomes

$$S = S_1 + S_2 - 1$$

If either surface is black (emissivity of one), the overall shielding factor is equal to that of the non-black surface.

7.1.1. Test Results

The thermal balance equation of the patch in the test fixture is

$$\sigma \epsilon_p A_p (T_p{}^4 - T_o{}^4) = \frac{\sigma A i}{2} \epsilon_g (T_b{}^4 - T_p{}^4) + K_p (T_b - T_p) + \Phi_h + \Phi_s$$

where

- ϵ_p = effective emissivity for interchange between front of patch and cold target
- ϵ_g = emissivity of gold plated surfaces on rear of patch and base
- A_p = front (black) area of patch
- A_i = side and bottom (gold) area of patch
- T_p = patch temperature
- T_o = cold target temperature
- T_b = base temperature
- Φ_h = joule heat on patch
- Φ_s = radiative input from support shields

An approximate formula for Φ_s is derived in Section 7.1.2 in terms of the shield emissivity ϵ_s, the support outer area A_s, and the temperature T_b and T_p. Because of the approximate nature of the formula for ϵ_s, we will assume that ϵ_s equals ϵ_g and therefore obtain an average emissivity for all gold surfaces. In addition, we will use a value of ϵ_p (0.89) based on a previous determination of the black paint emissivity (first quarterly report, Section 4.2). A variation of ±0.03 in ϵ_p results in a variation of about ± 6 percent in ϵ_g, comparable with the variation in the experimental results.

The thermal conductance K_p is equal to 0.0407 mW/K. The conductive paths are those through the two synthane supports (1/8 inch O. D. and 3/32 inch I. D.), two chromel heater leads (3×10^{-3} inch diameter), and two chromel-constantan thermocouple leads (3×10^{-3} inch). The length of all paths is 2.5 inches.

The test measurements are listed in Table 7-1. Each temperature is the average of from four to six readings taken after thermal equilibrium had been reached.

Table 7-1
Test Measurements

Test No.	T_b	T_p	T_o	Φ_h
1	300.4	149.7	85.6	25.286
2	301.0	158.3	86.8	52.692
3	301.1	141.5	87.0	0

Temperature in kelvins; power in milliwatts.

For the set-up used,

$$A_p = 5.944 \text{ in}^2$$
$$A_i = 6.822 \text{ in}^2$$
$$2A_s = 1.963 \text{ in}^2$$

The calculated values of gold surface emissivity (ϵ_g) are listed in Table 7-2 for an effective patch emissivity (ϵ_p) of 0.89.

Table 7-2
Emissivity of Gold Surfaces

Test No.	ϵ_g
1	0.0422
2	0.0401
3	0.0445
Average	0.0423

7.1.2 Radiative Input to Supports

The geometry of a patch support and its coaxial shield is shown in Figure 7-1. We will assume a linear temperature distribution between the base and patch. In addition, we will assume that all the net radiative input to the outer surface of the support is conducted into the patch. An area element on the outer surface of the support at a distance x from its connection to the base, absorbs a net radiant power given by

$$d\Phi x = \pi D \epsilon_s \sigma (T_b{}^4 - T \quad {}^4)\, dx$$

where D is the other diameter of the support, ϵ_s the emissivity of the shield, and T_x the temperature at X. The support is assumed to be black.

For the linear temperature drop, we have

$$Tx = T_b - (T_b - T_p)\frac{x}{\ell}$$

where ℓ is the lenght of the support between the base and patch. Inserting this into the expression for $d\Phi x$ and integrating from 0 to ℓ, we obtain the radiant power absorbed in the outer surface of the support tube.

Simplifying and rearranging, we obtain an expression for the radiative input to the support,

$$\Phi_s = \sigma A_s \epsilon_s (T_b{}^4 - T_p{}^4)\left[\frac{T_b}{T_b + T_p} - \frac{(T_b - T_p)^4}{5(T_b{}^4 - T_p{}^4)}\right]$$

where A_s is the outer support area, $\pi D \ell$. At the temperatures measured, the expression within the square brackets has a value of 0.654 ± 0.010 and is therefore very nearly constant.

A = SUPPORT
B = GOLD SHIELD

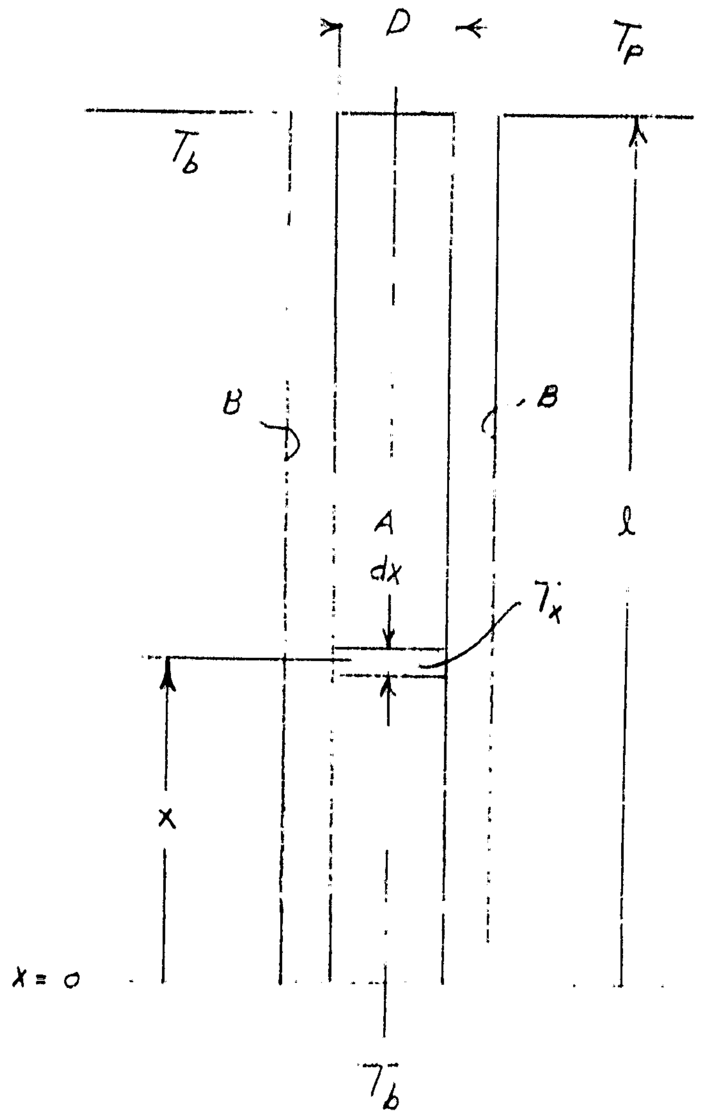

Figure 7-1 Patch Support and Coaxial Shield

7.2 Bell Jar Emissometer

The space chamber used for the experimental studies will be modified to allow the measurement of the hemispherical emissivity of flat samples. The technique utilized is basically a calorimetric one in which the sample temperature is fixed. It is described in detail in Part II to the final report on Contract NAS5-11683 (8 April - 15 December 1969). The honeycomb liquid nitrogen target was modified to a shallow cylindrical cold cavity by the addition of a honeycomb skirt. A measuring plate or disk was constructed of aluminum foil and honeycomb. It will be suspended from the cold cavity by means of two thermocouple leads and two additional support wires. The sample (cone wall) wil be attached to a temperature regulated baseplate. The sample base will permit the measurement of a wide range of wall sizes and shapes (Figure 7-2).

The basic equation of the experiment relates the emissivity of the sample (ϵ_1) to the measured temperatures of the sample (T_1), measuring plate (T_2), and cold cavity (T_3). For only radiative coupling between surfaces and for thermal equilibrium, the equation is (Section 2.0 of the above report).

$$\epsilon_1 = 0.95 \frac{T_2^4 - T_3^4}{T_1^4 - T_2^4}$$

This result holds for a low emissivity sample ($\epsilon_1 << 1$) and for honeycomb facing honeycomb between the disk and cavity. Both sides of the disk and the cavity are assumed to be covered with black paint whose emissivity is 0.91 (first quarterly report, Section 4.2).

For T_1 = 300K and T_3 = 85K, T_2 = 121.5K when ϵ_1 = 0.02. The net power emitted (or received) by the disk is

$$\Phi_{2-3} = 0.95 (T_2^4 - T_3^4) \sigma A_2,$$

where A_2 is the high emissivity area of either side of the disk (the sides of the disk are covered with low-emissivity material as described in Part II of the final report on Contract NAS5-11683). The disk has a 1.50 inch diameter, so that for the above temperatures, it radiates a net thermal equilibrium power of 10.19 mW. If the supports are to conduct no more than 2 percent of this amount (corresponding to a 2 percent error in the emissivity measurement; Section 4.3 of the above report), their thermal conductance cannot exceed

$$K_W = \frac{2.04\times10^{-4}}{36.5} = 5.59\times10^{-6} W/K$$

The support wires will all be 2 inches long between the disk and cavity. They will consist of three chromel and one constantan, all 3×10^{-3} inch in diameter. The resultant thermal conductance is 5.57×10^{-6} W/K.

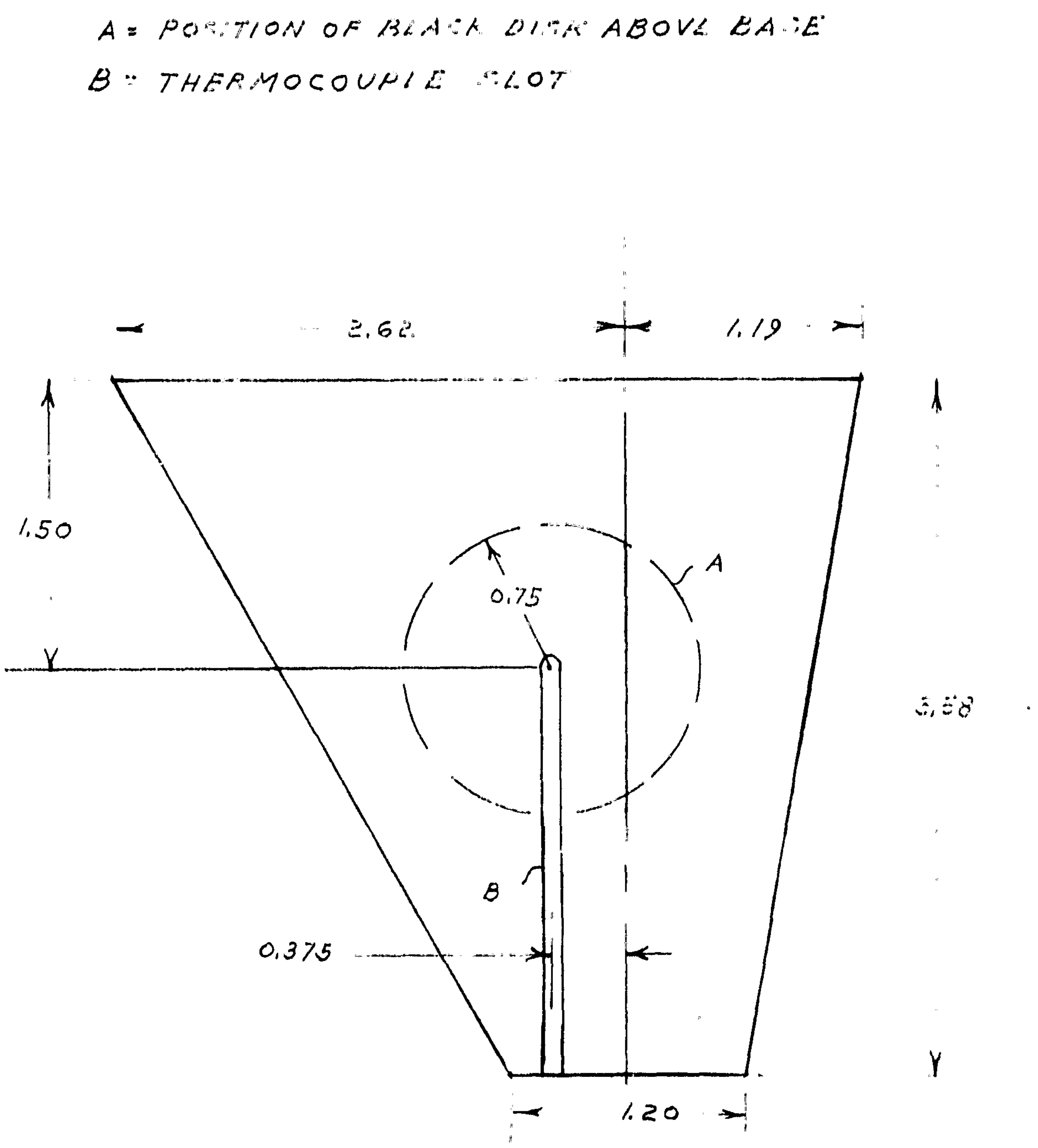

Figure 7-2 Cone Wall Base for Emissiometer (Dimensions in inches)

8.0 NEW TECHNOLOGY

No items which are considered new technology according to NASA form 1162 were developed during the second quarter of the second contract phase.

9.0 PROGRAM FOR NEXT PERIOD

The program will be completed before the end of another quarter. Specifically, the modified schedule calls for delivery of the breadboard cooler on or before 19 May 1971.

APPENDIX

SINUSOIDAL VIBRATION TEST

ON THE DUAL PATCH ASSEMBLY

ITT AEROSPACE/OPTICAL DIVISION
ELECTRO-OPTICAL OPERATIONS
Fort Wayne, Indiana

ENVIRONMENTAL TEST LABORATORY

January 14, 1971 Report No. 1577

1.0 DESCRIPTION

1.1 One (1) Merc Patch was submitted to the test laboratory for a vibration test.

2.0 PROCEDURE

2.1 The Merc Patch was mounted by its normal mounting means to an aluminum fixture (see Fig. I).

2.2 The unit was subjected to harmonic motion along each of three mutually perpendicular axes. The frequency range from 5 to 2000 Hz was traversed one time in each axis at a sweep rate of one octave per minute. The amplitude of motion was 0.10 inch D.A. or 20 G's whichever was less.

2.3 During the sweep in each axis resonant frequencies were noted.

2.4 Total vibration time for the three axes was approximately 30 minutes.

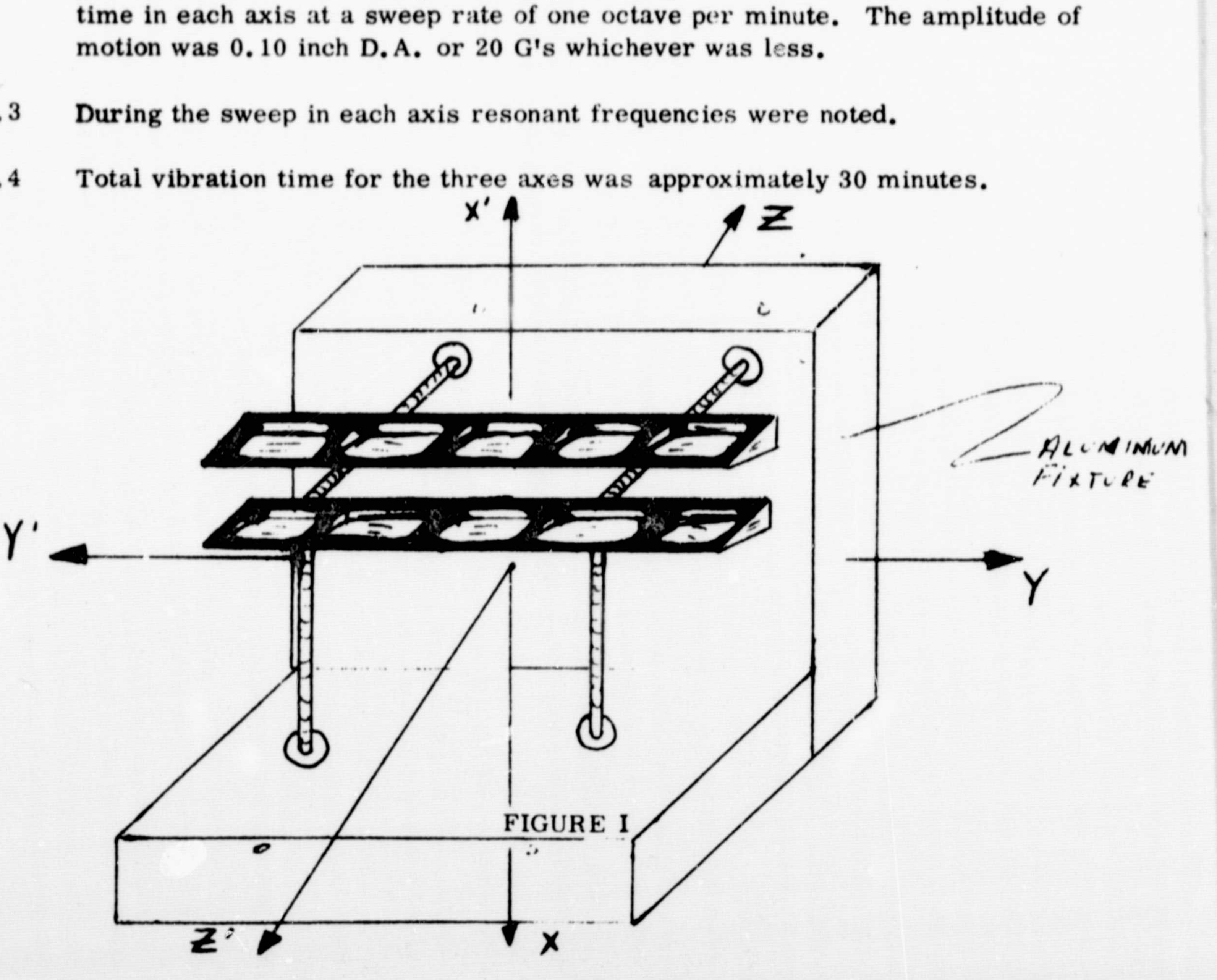

FIGURE I

3.0 RESULTS

3.1 One of the four horizontal supporting rods cemented to the Merc Patch came loose after completing vibration in the Y axis. The rod was re-cemented and the Z axis vibration test was completed without incident.

3.2 Resonance frequencies were noted in each of the following axes.

X-Axis	Y-Axis	Z-Axis
105 Hz	30 Hz	80 Hz
	85 Hz	100 Hz

4.0 NOTES

4.1 Test requested by J. Lodder, Industrial Park.

4.2 Test completed on January 11, 1971.

4.3 Test performed by E. G. Stark.
E. G. Stark